Journal of Physics: Conference Series

PAPER • OPEN ACCESS

The effect of time delay on control stability of an electromagnetic active tuned mass damper for vibration control

To cite this article: A Hassan *et al* 2016 *J. Phys.: Conf. Ser.* **721** 012007

View the article online for updates and enhancements.

Related content

- Analysis on Control Stability of STATCOM Applied on Weak Power System
  Taixun Fang, Yu Wang and Yeyuan Xie
- Effect of Time Delay on Binary Signal Detection via a Bistable System
  Zeng Ling-Zao, Liu Bing-Yang, Xu Yi-Da et al.
- Effects of time delay on stochastic resonance of a periodically driven linear system with multiplicative and periodically modulated additive white noises
  Du Lu-Chun and Mei Dong-Cheng

IOP ebooks™

Bringing you innovative digital publishing with leading voices to create your essential collection of books in STEM research.

Start exploring the collection - download the first chapter of every title for free.

This content was downloaded from IP address 151.224.127.146 on 08/04/2019 at 18:48

The effect of time delay on control stability of an electromagnetic active tuned mass damper for vibration control

A Hassan, A Torres-Perez, S Kaczmarczyk, P Picton

The University of Northampton, St. George's Avenue, Northampton, NN2 6JD, United Kingdom

Ali.hassan@northampton.ac.uk

Abstract. The aim of this paper is to investigate the effect of time delays on the stability of a zero-placement position and velocity feedback law for a vibratory system comprising harmonic excitation equipped with an electromagnetic active tuned mass damper (ATMD). The purpose of the active control is broadening the vibration attenuation envelope of a primary mass to a higher frequency region identified as from 50±0.5Hz with a passive tuned mass damper (TMD) to a wider range of 50±5Hz with an ATMD. Stability conditions of the closed-loop system are determined by studying the position of the system closed-loop poles after the introduction of time delays for different excitation frequencies. A computer simulation of the model predicted that the proposed control system is subject to instability after a critical time delay margin dependent upon the frequency of excitation and the finding were experimentally validated. Three solutions are derived and experimentally tested for minimising the effect of time delays on the stability of the control system. The first solution is associated with the introduction of more damping in the absorber system. The second incorporates using a time-delayed ATMD by tuning its original natural resonant frequency to beyond the nominal operational frequency range of the composite system. The third involves an online gain tuning of filter coefficients in a dual arrangement of low-pass and high-pass filters to eliminate the effect time delays by manipulating the signal phase shifts

1. Introduction

The motivation of this work arises from the vibration problem that arises within a free piston Stirling engine generator. Stirling engines are power machines that operate over a closed, regenerative thermodynamic cycle, with cyclic compression and expansion of the working fluid at different temperature levels [1]. The power piston inside the engine is fitted with a set of permanent magnets that oscillate inside the linear alternator to generate electrical current at 50Hz. Hence this type of grid connected machines is designed and tuned to operate within a frequency range of 50Hz ± 0.5Hz in Europe. The reciprocating movement of the power piston causes a vibration within the engine that can be intolerable. In general, the damping of vibration in equipment is usually accomplished by employing visco-elastic materials [2,3]. Currently, a passive TMD is employed to absorb the vibration coming from the piston at 50Hz. Recently the European Network of Transmission System Operators for Electricity (ENTSO) has brought new regulations for grid connection and disconnection of low power generation devices which introduced wider grid operation frequencies between 47-53Hz. The operation of the Stirling engine is affected by the new regulation since its passive TMD is originally tuned to cancel the vibration of the engine within a very narrow bandwidth. Active damping techniques can achieve far better performance than simple passive ones by employing actuators and complex control systems. The active control of vibration has gained some considerable level of attention in civil engineering and a number of successful implementation was achieved [4]. In [5], an active tuned mass damper that could be used to control lateral vibrations induced by pedestrians on a

Content from this work may be used under the terms of the Creative Commons Attribution 3.0 licence. Any further distribution of this work must maintain attribution to the author(s) and the title of the work, journal citation and DOI.
Published under licence by IOP Publishing Ltd

bridge deck was presented. The work was tested using a bridge model equipped with a prototype active mass damper. In recent years, there has been a growing interest in using electromagnetic actuators instead of piezoelectric actuators. In [6] a four-mount active vibration isolation system using voice coil actuators was developed. In [7] a voice coil actuator with velocity feedback control for highly sensitive instruments by producing a sky-hook damper at low frequencies (2-6 Hz) was considered. Their proposed method reduced the vibration at resonance without causing larger vibration amplitudes at higher frequencies.

Closed-loop control using structural displacement and velocity feedbacks for active vibration reduction is perceived as a common practice in vibration control. It is generally difficult to achieve accurate measurements of velocity and displacement directly in many systems particularly that lack inertial reference frames. Acceleration measurements, on the other hand, are practically easier to obtain without the requirement of a reference frame and with sensors featuring accurate and wide frequency band [8]. Numerical integration is often employed in order to obtain displacement and velocity measurement from acceleration signals, resulting in the appearance of DC offset component in the signal, particularly after the second integration action [9]. Anti-aliasing and noise filtering, as well as DC component elimination induce an inevitable group time delay that may affect in deterring the control performance and even causing instability [10].

In terms of active vibration control studies that bear attention to the effect of time delays, a method of active control based on time delay compensation for the low-order modes of a cantilever-like structure suffering from complex excitations was developed in [11]. The solution was based on constructing an autoregressive moving average (ARMA) model for eliminating the time delay caused by filters. A control system for a time-delayed active vibration absorber, which can eliminate the vibration of the primary structure subject to a sinusoidal disturbance was proposed and tested experimentally in [12]. Two kinds of controller design methods for active vibration control problem with input time delay, where the time-delayed system is first transformed into a delay-free system, so that the classical control strategies such as the LQR method can be applied directly was developed in [13]. In [14] a time-delayed acceleration feedback controller for the active vibration control of flexible structure was proposed. In [15] a study on the design of the acceleration-based active vibration control for flexible structures with bonded piezoelectric patches is presented, where by manipulating the phase shift, time delay compensation caused by non-collocated sensor/actuator pair is achieved.

The work done in [16] serves a basis for the study presented in this paper. The active vibration control of a structure using displacement and velocity feedback law to change the natural resonance and the damping in an ATMD is implemented using a test rig that utilizes a voice coil motor for an ATMD. A detailed theoretical study into the effect of time delays on the control stability is presented by studying the system poles with the introduction of delays. The theoretical findings and experimental realization illustrated that instability of the control system occurs beyond a critical time delay margin depending on the excitation frequency. Two solutions to mitigate the time-delay induced instability were proposed and experimentally verified. The first is based on using a time-delayed ATMD whilst shifting its original resonant frequency above the system's nominal frequency band of operation. The second solution is based on an online gain tuning of the coefficients of a dual filtering arrangement in order to manipulate the individual phase shifts of the two filters accordingly so that a time delay effect is eliminated. It was found that the first solution incurs the use of more electrical power than the second and the hence it was found to be 50% less efficient in terms of power consumption.

2. Test rig development

Following the results of the theoretical work that was carried out in [16], a scaled test rig was developed to demonstrate the concept of active damping with ATMD with particular emphasis on the effect of time delays on the proposed control strategy

2.1. Test rig system

In the test rig shown in **Figure 1**, an electrodynamic shaker (V406) from B&K is mounted vertically as shown. The shaker acts as the source of sinusoidal excitation to the 2-DOF system which features a shaker table whose vibration to be cancelled by means of an ATMD system that, in turn, is passively tuned at 50Hz. The ATMD consists of a planar spring attached to the top of the moving shaker table. A Voice Coil Motor (VCM) provides the actuation for active damping and is mounted between the shaker table and the dynamic mass of the ATMD. The vibration model of the test rig is also shown in **Figure 1** on the left. The detailed description of the model is presented in the following section.

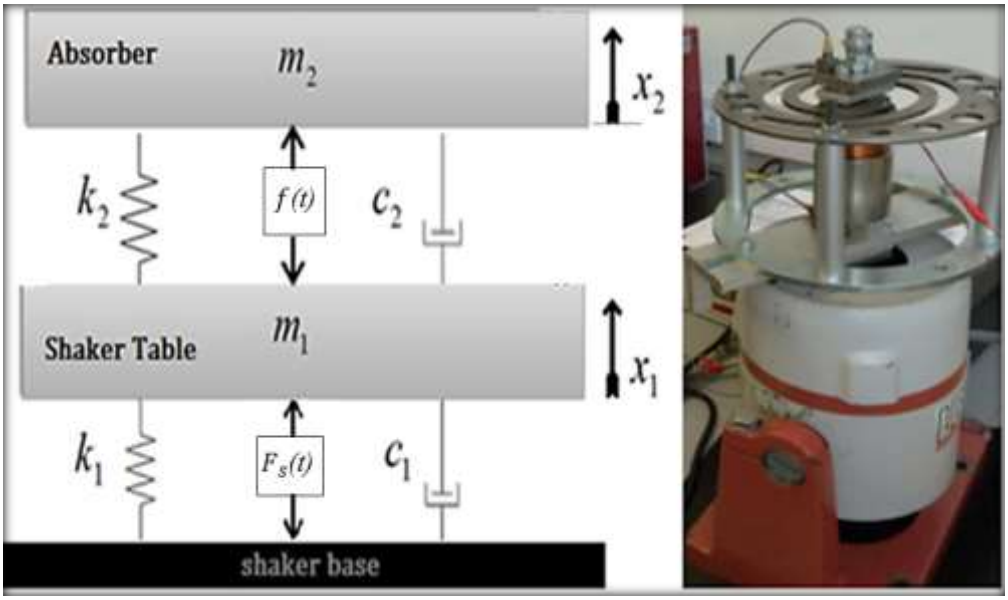

Figure 1. Test rig and the corresponding vibration model

2.2. Mathematical Model

An electromechanical model is developed to represent the shaker rig mathematically for the purpose of performing theoretical studies. The VCM is modelled as an RL circuit with V_a and i_a representing the voltage across and the current through the VCM terminals. The terms R_a, L_a, and k_a represent the motor coil inductance, resistance, and the motor constant respectively. The mass m_1 is the mass of the shaker table plus that of the VCM's stationary base and the absorber's stationary mass. The mass m_2 includes the dynamic mass of the absorber and the VCM's moving coil. Here it is assumed that the value of the back electromotive force (EMF) constant is the same as k_a. The control force f_a is proportional to the VCM motor current i_a by k_a. A proportional controller is used to control the VCM current i_a by comparing it to a desired current i_r . The excitation force F is generated by the dynamic shaker which has a similar model to the VCM represented with subscript s. The variable x_1 represents the shaker table displacement, x_2 the absorber mass displacement, $\dot{x}_1$ the shaker table velocity and $\dot{x}_2$ the absorber velocity. The resulting equations of the coupled electromechanical system are shown below

$$\begin{cases} m_1\ddot{x}_1 + k_1x_1 + c_1\dot{x}_1 + k_2(x_1 - x_2) + c_2(\dot{x}_1 - \dot{x}_2) = F_s - f_a \\ m_2\ddot{x}_2 + k_2(x_2 - x_1) + c_2(\dot{x}_2 - \dot{x}_1) = f_a \\ V_a = R_a i_a + L_a \dfrac{di_a}{dt} + k_a(\dot{x}_1 - \dot{x}_2) \\ V_s = R_s i_s + L_s \dfrac{di_s}{dt} - k_s\dot{x}_1 \\ F_s = k_s i_s \\ f_a = \beta(\dot{x}_1 - \dot{x}_2) + \gamma(x_1 - x_2) \\ i_r = f_a/k_a \\ V_a = k_p(i_r - i_a) \end{cases} \tag{1}$$

where γ and β are relative positon and relative velocity feedback gains for the zero placement control technique and derived as

$$\gamma = 4\pi^2\, m_2({f_{exc}}^2 - {f_0}^2) \qquad \text{and} \qquad \beta = -c_2 \tag{2}$$

f_{exc} is the excitation frequency and f_0 is the resonant frequency of the absorber. The stability condition of the control law is derived following the Routh-Hurwitz criterion [17]:

$$\alpha > -m_2 \qquad \beta > -c_2 \qquad \gamma > -k_2$$

For ATMD applications, maximum attenuation is achieved in the primary mass when the damping in the absorber is minimal; hence a negative velocity feedback gain equivalent to the damping coefficient of the absorber seems a perfect choice. However, by examining the stability condition of the control law, the velocity feedback gain β has to be greater than $-c_2$. Hence, to avoid a marginal stability situation, β is chosen slightly greater than $-c_2$ to achieve both, high attenuation level and stability. The following shows one of the possible state-space model representations of the 2-DOF system comprising the electrodynamic shaker and the ATMD.

$$\begin{bmatrix} \dot{x}_1 \\ \dot{x}_2 \\ \dot{x}_3 \\ \dot{x}_4 \\ \dot{x}_5 \\ \dot{x}_6 \\ \dot{x}_7 \\ \dot{x}_8 \\ \dot{x}_9 \end{bmatrix} = \begin{bmatrix} 0 & 0 & 0 & 0 & 1 & 0 & 0 & 0 & 0 \\ 0 & 0 & 0 & 0 & 0 & 1 & 0 & 0 & 0 \\ 0 & 0 & 0 & 0 & 0 & 0 & 1 & 0 & 0 \\ 0 & 0 & 0 & 0 & 0 & 0 & 0 & 1 & 0 \\ \frac{-(k_1+k_2)}{m_1} & \frac{k_2}{m_1} & 0 & 0 & \frac{-(c_1+c_2)}{m_1} & \frac{c_2}{m_1} & \frac{-k_a}{m_1} & \frac{k_s}{m_1} & 0 \\ \frac{k_2}{m_2} & \frac{-k_2}{m_2} & 0 & 0 & \frac{c_2}{m_2} & \frac{-c_2}{m_2} & \frac{k_a}{m_2} & 0 & 0 \\ 0 & 0 & 0 & 0 & \frac{k_a}{L_a} & \frac{-k_a}{L_a} & 0 & 0 & \frac{1}{L_a} \\ 0 & 0 & 0 & 0 & -\frac{k_s}{L_s} & 0 & 0 & \frac{-R_s}{L_s} & 0 \\ 0 & 0 & 0 & 0 & 0 & 0 & 0 & 0 & 0 \end{bmatrix} \begin{bmatrix} x_1 \\ x_2 \\ x_3 \\ x_4 \\ x_5 \\ x_6 \\ x_7 \\ x_8 \\ x_9 \end{bmatrix} + \begin{bmatrix} 0 & 0 \\ 0 & 0 \\ 0 & 0 \\ 0 & 0 \\ 0 & 0 \\ 0 & 0 \\ 0 & \frac{-R_a}{L_a} \\ \frac{1}{L_s} & 0 \\ 0 & 0 \end{bmatrix} \begin{bmatrix} V_s \\ i_a \end{bmatrix} \tag{3}$$

The following define the state-space variables

$x_1 = shaker\ table\ displacement \quad x_2 = absorber\ displacement \quad x_3 = electrical\ charge\ in\ the\ VCM$
$x_4 = electrical\ charge\ in\ the\ shaker\ coil \quad x_5 = shaker\ table\ velocity \quad x_6 = absorber\ velocity$
$x_7 = VCM\ current \qquad x_8 = shaker\ current \qquad x_9 = VCM\ voltage$

2.3. Model simulation and validation

In this section, the model of the test rig is simulated in the frequency domain and the results are plotted against the experimental results. The values of Table 1 are adopted for the model simulation and test parameters of the rig.

Table 1. Model Simulation parameters

Parameter	Value	Unit	Parameter	Value	Unit
m_1	2.1	[kg]	V_s	3sin(2πft)	[V]
m_2	0.403	[kg]	L_s	1.8	[mH]
c_1	1	[Ns/m]	R_s	1.2	[Ω]
c_2	7	[Ns/m]	k_s	11.1	[N/A]
k_1	12300	[N/m]	L_a	1.3	[mH]
k_2	39775	[N/m]	R_a	2.7	[Ω]
f_{exc}	5-100	[Hz]	k_a	8	[N/A]

In the experiment the VCM is not powered and the leads are left open- that is to say that there is no control operation throughout this test. The test is carried using a sinusoidal excitation with variable frequency of the shaker between 5Hz and 100Hz in open loop. Two accelerometers of 100 mv/g sensitivity and 70g max dynamic range were used to collect data from both the absorber and shaker table accelerations. In addition to that, the electrical current consumed by the shaker is measured using a low noise non-contact current of dynamic range $\pm 20A$ and 0.01 A resolution. The results from both the simulation and experiments are depicted in the graphs of Figure 2.

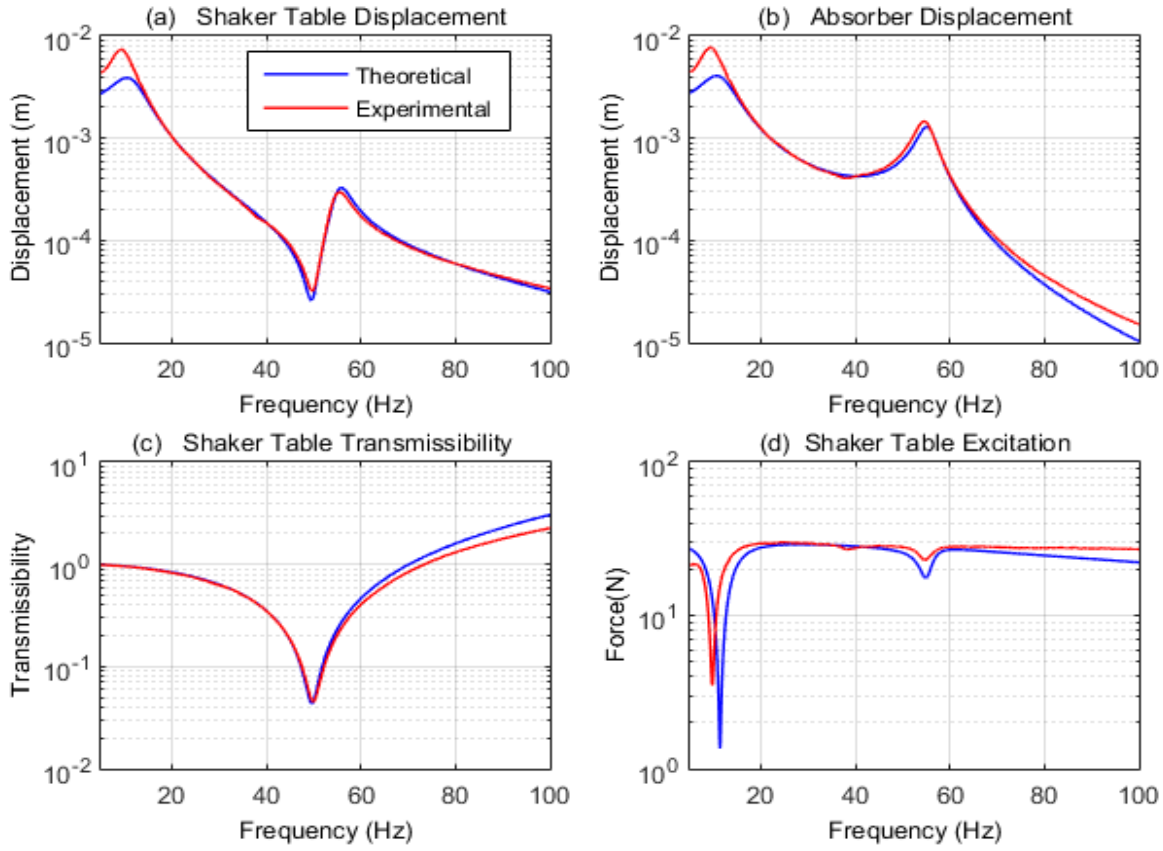

Figure 2. Theoretical model results vs experimental results. The value of damping coefficient is determined $c_2 = 7\ NS/m$

The results reveal a very close match between the theoretical model predictions and the experimental results. Figure 2 (a) shows the curves of the shaker table displacement with two peaks corresponding to the resonant frequencies of the composite at 10Hz and 55Hz. At 50Hz, the shaker displacement is attenuated to minimum due to the effect of the anti-resonant frequency of the TMD. The transmissibility to the shaker table is shown in (c) and reveals that at 50Hz, the shaker force is completely transmitted from the shaker table to the absorber mass. The experimental results revealed the VCM introduces damping into the ATMD system and the value of the damping is determined as $c_2 = 7\ Ns/m$ following graph reverse fitting of the theoretical results onto the experimental ones.

3. Time delays

3.1. Expression of the actuator force with time delays

The intention of this section is to represent actuator force with the time delay term embedded in it. This analysis considers the zero-placement control law with position and velocity feedback for the active control. A time delay $d(t-\tau)$ can be expressed by $e^{-\tau s}$ in the Laplace domain with τ defined as the amount of time delay. To make it possible for studying the poles of the transfer function, the exponential term of the delay has to be transformed into a rational form. The first order Taylor approximation assuming a sinusoidal force of period T in the frequency domain becomes

$$e^{-\tau s} \approx 1 - \tau s \tag{4}$$

The form of the delayed actuator force can be expressed as follows

$$f_a(t-\tau) = d(t-\tau)[\beta(\dot{x}_1 - \dot{x}_2) + \ \gamma(x_1 - x_2)] \tag{5}$$

Equation (5) is incorporated into the system model presented in system of equations (1) to account for delays in the system. While ignoring the shaker dynamics, the resulting transfer function from shaker excitation force to the shaker table displacement can expressed in the Laplace domain as follows

$$W(s) = \frac{X_1(s)}{F_s(s)} = \frac{b_3 s^3 + b_2 s^2 + b_1 s^1 + b_0}{a_4 s^4 + a_4 s^4 + a_3 s^3 + a_2 s^2 + a_1 s + a_0} \tag{6}$$

The coefficient of the numerator and the denominator of $W(s)$ are shown in *Appendix A*. The roots of $W(s)$ are studied and the real part of the closed-loop poles are investigated for different time delays as the excitation frequency is varied. The simulation was carried out for time delays between 0s and 200μs and excitation frequency between 45Hz and 55Hz. The values of **Table 1Error! Reference source not found.** are adopted for this simulation. The position gain γ and velocity gain β are calculated as per equation (2). Figure 3 below shows the variation of the real part of the closed-loop poles. The horizontal axis of each subplot represents that of the time delay in seconds and the vertical axis represents the real part of the poles. The imaginary part is ignored and only the real part of the system poles is considered. This analysis is similar to the conventional root-locus analysis but it doesn't consider the imaginary part. In fact it is not possible to perform this analysis with the conventional root-locus method because each value of time delay corresponds to a different transfer function $W(s)$.

The results presented below show that all the system poles have negative real parts for time delays between 0s and 200μs for excitation frequencies below 50Hz indicating to system stability. As the excitation frequency moves above the original resonance of the ATMD (50Hz), the control system becomes unstable shortly after a certain delay margin which decreases consistently with the increase in the excitation frequency.

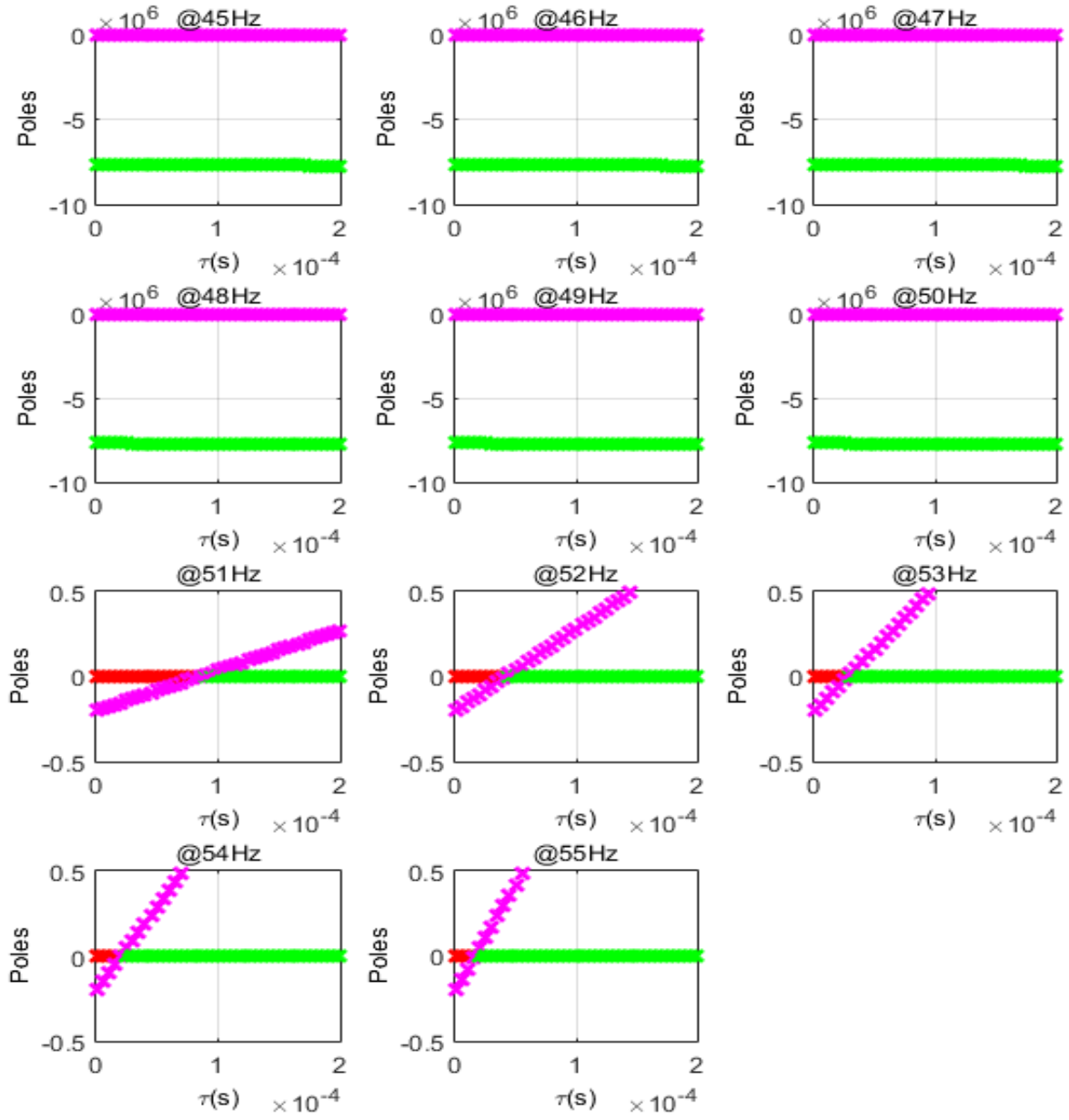

Figure 3. Plots showing the variation of the real part of the system poles as a function of time delay and excitation frequency with ATMD tuned at 50Hz with damping removed completely.

3.2. Solution 1: Change of damping in the ATMD

Another important observation is made concerning the relation between the critical time delay margin and the damping in the ATMD. The theoretical analysis shows that allowing a little more damping in the absorber improves the delay time margin as depicted in **Figure 4**. In this simulation, the velocity feedback gain beta was chosen to be $\beta > -c_2$ for the purpose of allowing more damping in the ATMD system. The results of this simulation are plotted in **Figure 4**. It is shown that when a little damping is allowed in the system, time delay still affect system stability however the time delay margin is longer at each particular frequency above 50Hz compared to **Figure 3**. While allowing more damping in the ATMD would eventually increases the stability margin, there exists an inverse trade-off between the amount of damping that is allowed in the ATMD and level of attenuation achieved in the vibration of the structure.

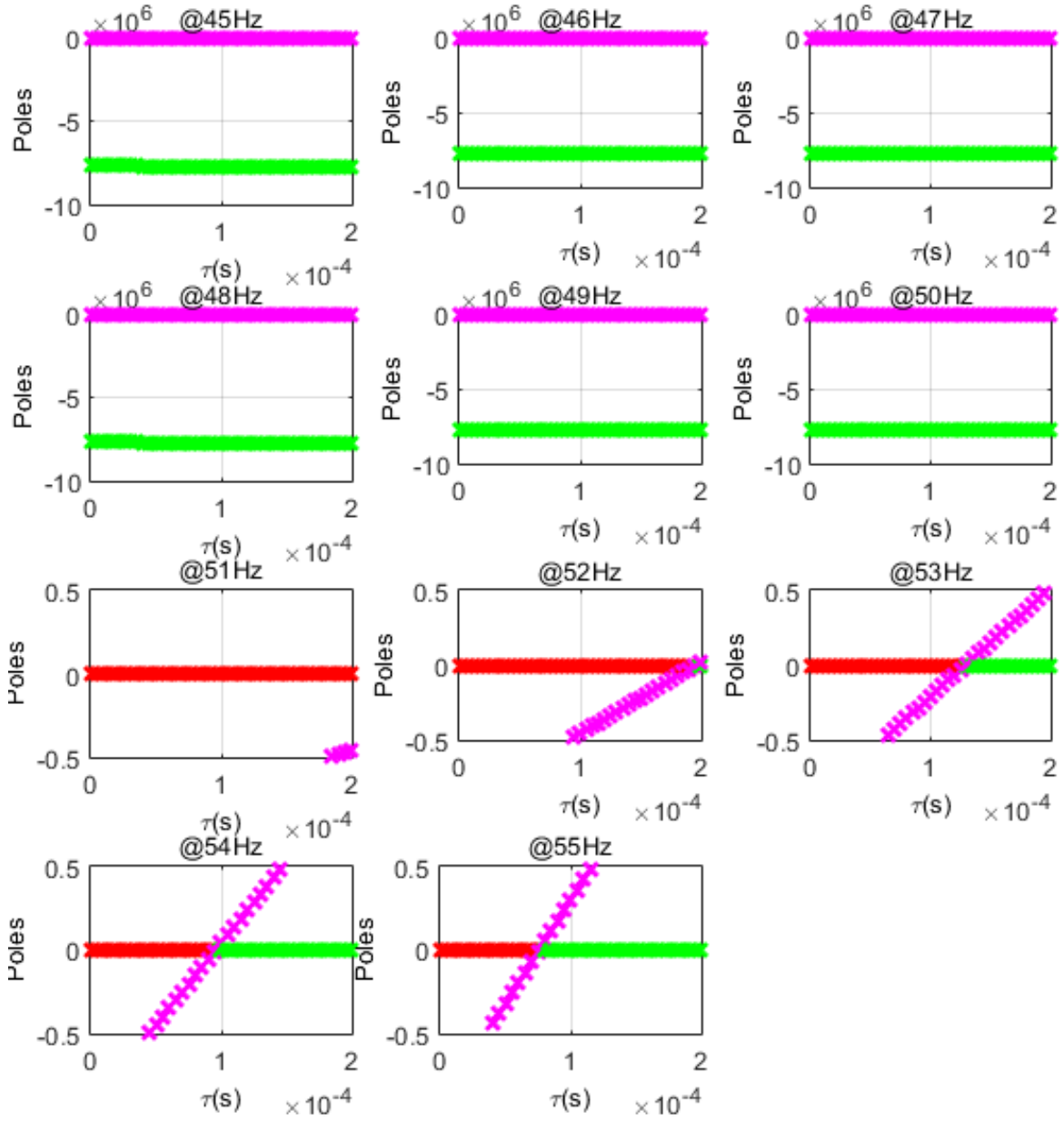

Figure 4 System poles variation as a function of time delay and excitation frequency with ATMD tuned at 50Hz with some damping allowed in the ATMD

3.3. Solution 2: Change of ATMD original resonance

By recalling that the nominal operational frequency range of the system is between 45Hz-55Hz, and by noticing that the system becomes unstable for time delay margins for excitation frequencies above the original tuning of the absorber, a solution can be formulated based on shifting the original tuning of the ATMD is shifted to a frequency higher than the original resonance 55Hz and outside the nominal frequency range of the engine operation, the system is guaranteed to be stable when the frequency of excitation is below the 55Hz. A new simulation is carried out to check the stability when the ATMD resonance is moved to 55Hz. The results are shown in Figure 5 and reveal that this technique succeeds in mitigating the effect of delays on stability.

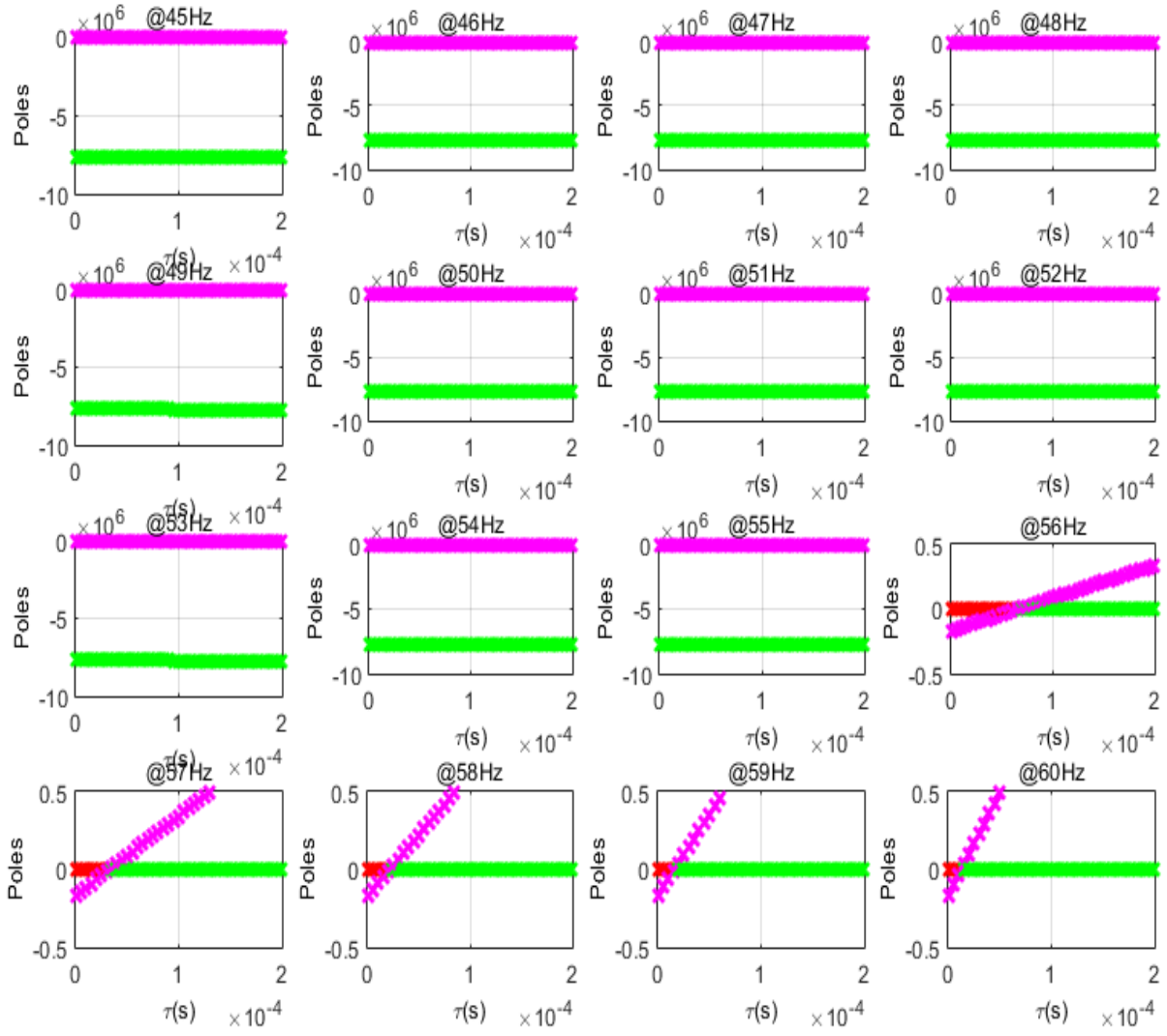

Figure 5. System poles variation as a function of time delay with 55Hz ATMD tuning

3.4. Discussion

While both of the techniques presented in the previous sub-sections serve as a successful mitigation solution of the time delay effect on stability of the control, there exist two main drawbacks that arise with following these approaches concerning efficiency and power consumption. The first technique works on the basis of increasing the time delay stability margin (time-delayed ATMD) by allowing for more damping in the system. Assuming the system has inherent damping such as the VCM, this technique is a feasible however a compromise on the level of attenuation of the shaker table vibration is made. The second technique also benefits from the design of a time-delayed ATMD, however damping can be removed from the system and hence maximum attenuation is possible. The main drawback with the second method arises from the perspective of power consumption since if the ATMD was originally tuned at 55Hz the position gain γ would be larger than the case when the ATMD was originally tuned at 50Hz as shown in and consequently more force is needed to actively shift the frequency of the ATMD.

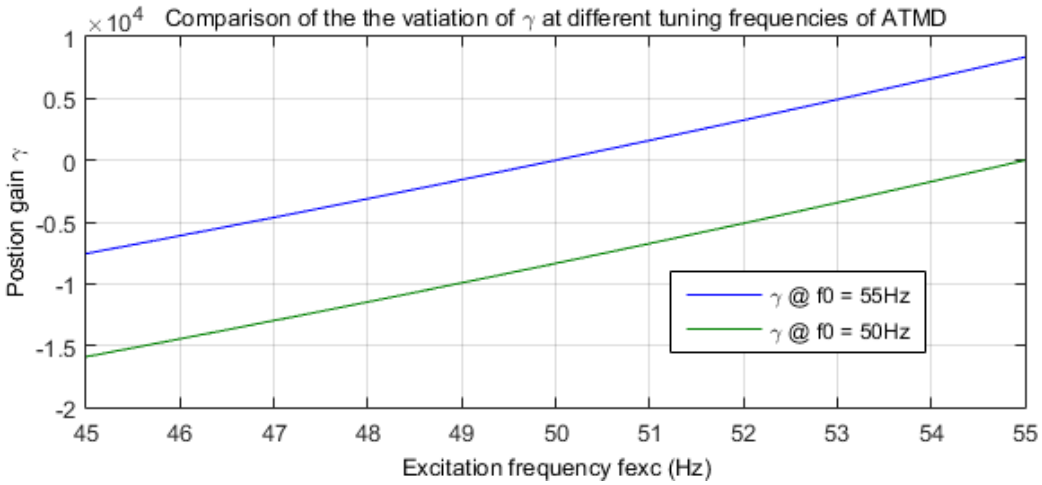

Figure 6. Position gain as a function of excitation frequency for two different ATMD resonant frequencies

3.5. Solution 3: Dual-filtering phase compensation

By recognizing the strengths and limitations of the previous two techniques, another method is proposed in this section for mitigating the effect of time delays on stability of the control system. The system under study is a linear-time invariant system with sinusoidal excitation and the steady-state of this system is assumed to be well known. In practice, the control implementation generally requires filtering of input signals for noise avoidance, anti-aliasing, and for DC component elimination. These induce inevitable group time delay that was shown earlier to affect stability of the control system. Furthermore, sensor measurement as well as non-collocated sensor/actuator pair in addition to processing times can induce more time delays. Reasons for these delays are geometrical arrangements, and computational time in analog digital converters (ADCs) and in digital analog converters (DACs). The delays represent a phase shift in periodic signals that obstruct instantaneous feedback of the signals. Phase shift manipulation can be also utilized for time delay compensation as per the following explanation. Assuming that a 2nd order Butterworth low-pass filter with 200Hz cut-off frequency is used for noise filtering and anti-aliasing, the continuous Laplace domain transfer function that represents the filter plant, $TF_{LP}(s)$, is shown below

$$TF_{LP}(s) = \frac{0.0001551s^2 + 15.7s + 1.579e06}{s^2 + 1777s + 1.579e06} \tag{7}$$

The phase angle equation of a 2nd order Butterworth filter is determined using the following equation

$$\emptyset_{LP}(f_{exc}) = -\tan^{-1}\left[\frac{1}{\zeta}\left(2\frac{f_{exc}}{f_{LP}} + \sqrt{4-\zeta^2}\right)\right] - \tan^{-1}\left[\frac{1}{\zeta}\left(2\frac{f_{exc}}{f_{LP}} - \sqrt{4-\zeta^2}\right)\right] \tag{8}$$

where f_{LP}, f, and ζ are the cut-off frequency, the excitation frequency, and the damping ratio of the filter respectively. The frequency response of the above filter is plotted in **Figure 7**. The intention is to illustrate the induced phase shift between 45Hz and 55Hz.

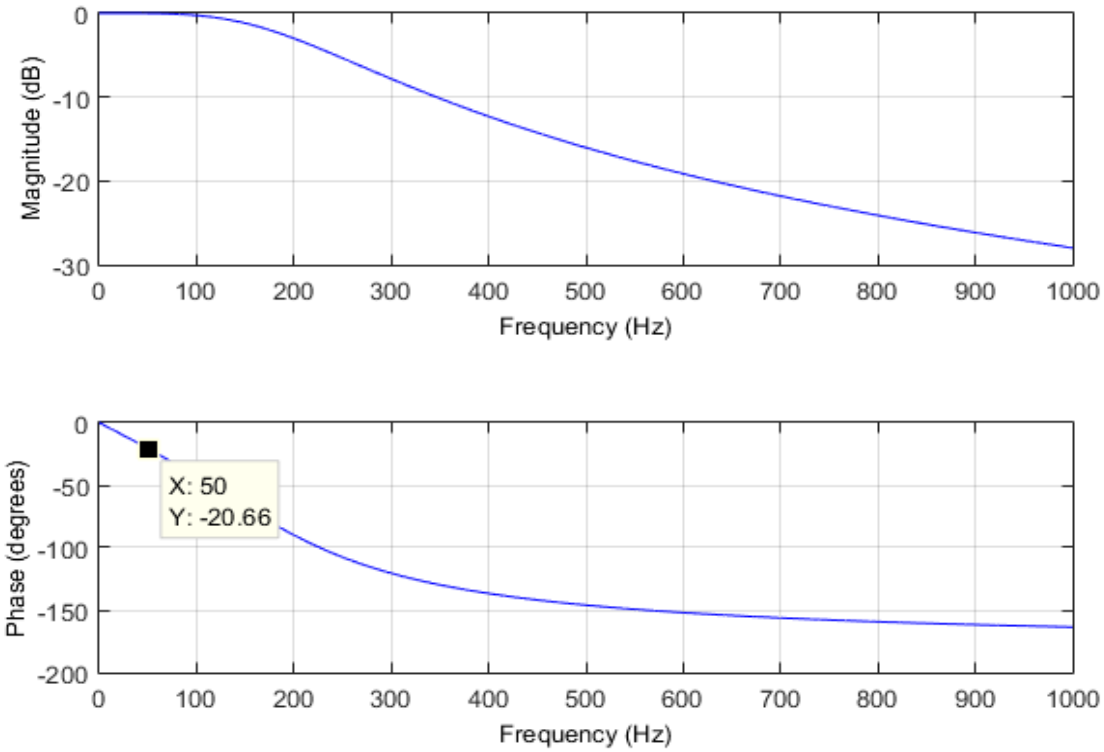

Figure 7. Low-pass Butterworth filter frequency response with cut-off frequency of 200Hz

Referring to the phase angle plot in the frequency range of 45-55Hz, the phase angles at 45Hz and 55Hz are -18.53^0 and -22.82^0 respectively. Those two phase shifts are associated with positive time delays of 1.143ms and 1.152ms at 45Hz and 55Hz respectively in accordance with the following relationship that associates time delay (τ) in second, the phase shift ($\emptyset$) in degrees, and the excitation frequency f_{exc}

$$\tau = \frac{\emptyset^0}{360^0 \times f_{exc}} \tag{9}$$

The phase shifts introduced by the low pass filter with 200Hz cut-off frequency have the effect of a time delay with a minimum value of 1.143ms at 45Hz and a maximum of 1.152ms at 55Hz.
Another kind of phase shift is now illustrated with the use of a 2nd order high-pass Butterworth filter with 1Hz cut-off frequency for the purpose of DC component elimination. The continuous Laplace domain transfer function that represents the filter plant, $TF_{Hp}(s)$, is shown below

$$TF_{HP}(s) = \frac{s^2 - 0.0003948s - 7.792e - 08}{s^2 + 8.886s + 39.48} \tag{10}$$

The phase angle equation of the 2nd order High-Pass Butterworth filter is determined using the following equation

$$\emptyset_{HP}(f_{exc}) = \pi - \tan^{-1}\left[\frac{1}{\zeta}\left(2\frac{f_{exc}}{f_{HP}} + \sqrt{4-\zeta^2}\right)\right] - \tan^{-1}\left[\frac{1}{\zeta}\left(2\frac{f_{exc}}{f_{HP}} - \sqrt{4-\zeta^2}\right)\right] \tag{11}$$

The phase equation for the high pass filter is similar to that of the low passes one advanced by a π radian. This means that while the Low-Pass filter corresponds to lagging the output signal, the High-Pass filter is associated with leading the output signal. The frequency response of the High-Pass filter used in the code is depicted in **Figure 8**.

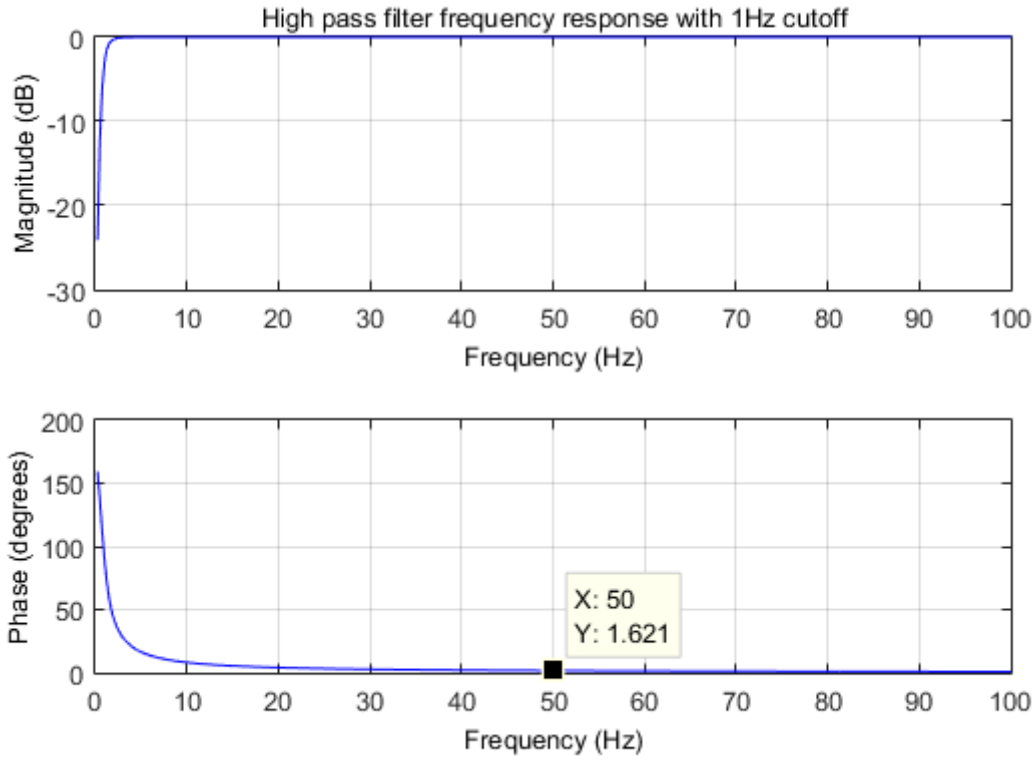

Figure 8. High-pass Butterworth filter frequency response with cut-off frequency of 1Hz

The phase angles at 45Hz and 55Hz are $1.801^0$and 1.473^0 respectively. Those phase shifts contribute to a max reverse time delayed output signal of -0.10006ms at 45Hz and min reverse time delay -0.07439ms at 55Hz. The group delay induced by the filtering stages is then estimated by adding the individual delays of each filter. Referring to the time delay margin identified in the investigation of the effect of time delays on control stability earlier, a careful choice of the cut-off frequencies of the low-pass and high-pass filters is capable of compensating the incurred group delays. The following discusses the derivation of the phase shift relationship between the High-Pass and Low-Pass filters cut-off frequencies. The aim is to obtain an analytic solution that relates the cut-off frequencies to the phase shift and then solve it to obtain a zero group phase shift. By adding the phase equations of the phase shift and equating to zero, the following equality is obtained

$$\frac{\zeta f_{exc}(f_{HP}+f_{LP})\left(-{f_{exc}}^2+f_{HP}f_{LP}\right)}{\zeta^2{f_{exc}}^2f_{HP}f_{LP}-(f_{HP}f_{LP})^2+(f_{exc}f_{HP})^2+(f_{exc}f_{LP})^2-{f_{exc}}^2}=0 \tag{12}$$

Assuming that cut-off frequency of one filter is known, the following shows the non-trivial solution that relates the excitation frequency to the cut-off frequencies

$${f_{exc}}^2=f_{LP}f_{HP} \tag{13}$$

4. Implementation

This section is dedicated to the validation of the findings presented in the previous section. In the experiments, the shaker is powered by a 1.3 KVA power amplifier which is controlled by a small voltage signal between ±2 volts. The VCM (GVCM-051-051-01) is powered and controlled with a servo linear drive amplifier TA105 capable of delivering a max current of 2A peak to peak control by a fast proportional current controller. During operation, the active damping control method determines a reference current that is fed to the servo drive and then compared with the actual current in the VCM which is measured internally. An embedded CompactRio 9024 controller featuring an industrial 800

MHz real-time processor that runs LabVIEW for deterministic, reliable real-time applications is used for control, logging, and data analysis. The CRIO also features a user-defined FPGA circuitry in its chassis that controls each I/O module. Two LabVIEW codes were implemented simultaneously on the Compact Rio's real time engine and the FPGA respectively. The FPGA code is executed with a 20μs loop rate where the measurement and control takes place. The RT code runs with a 100ms loop rate and communicates to the FPGA code via direct memory access FIFOs. Two analogue input modules (NI 9234, NI 9205) and one analogue output module (NI 9263) were used to process the signals. Acceleration data of the shaker table and the TMD were obtained from two accelerometers with dynamic range of ±71g mounted in the middle of the shaker table and the helical spring respectively. The acceleration signals were sampled at a rate of 50KS/s using an AC coupled input stage of a 24-bit Analogue-to-Digital converter. A low-pass filter with a cut-off frequency of 200Hz is employed to remove any measurement noise from the accelerometers.

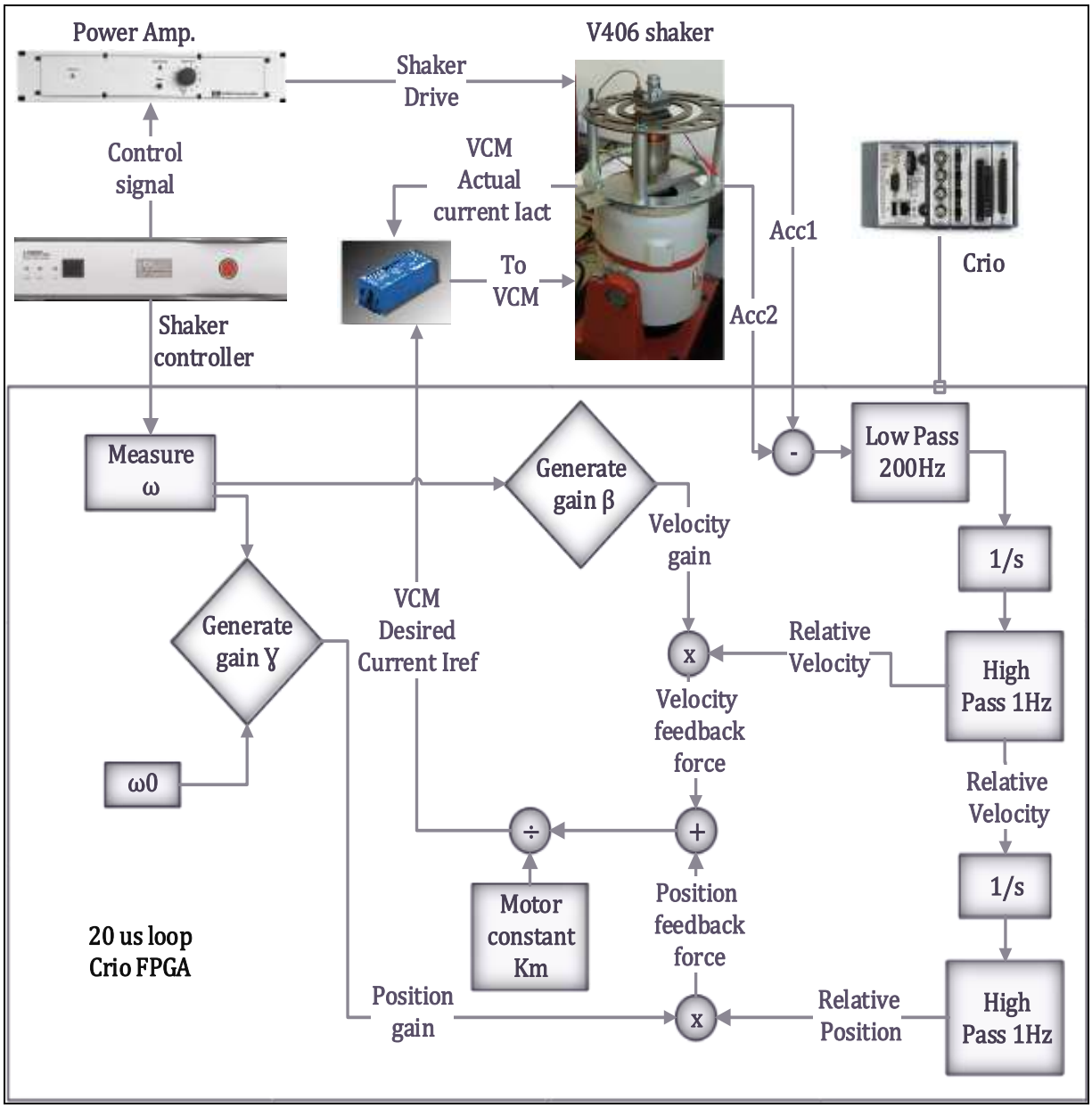

Figure 9. Schematic of the active damping control of Test 1 and Test 2

4.1. Test 1: Effect of induced time delays

In this test, the shaker excitation frequency is varied linearly from 40Hz to 60Hz in a time interval of 1 minute. The active vibration control is only operated in the frequency range between 45Hz and 55Hz. The ATMD is tuned at 50Hz and the active control aims to re-tune the ATMD frequency so it tracks that of the excitation and consequently cancel the vibration of the shaker table. Time delays of 1.143ms and 1.152ms are introduced between 45Hz and 55Hz by means of a second order Butterworth low-pass filter with 200Hz cut-off frequency that is originally used for noise and anti-aliasing. On the other hand, two High-Pass second orders Butterworth filters are implemented with a 1Hz cut-off frequency to remove any post-integration DC offset. The test parameters are summarized in **Table 2**. The value of the velocity feedback gain was chosen β = -14 Ns/m to remove the damping introduced from the VCM when the terminals are VCM are closed.

Table 2. Parameters for Test 1 and Test 2

Parameter	Symbol	Value	Unit
Shaker Excitation	V_s	$4\ \sin 2\pi f_{exc} t$	[V]
Excitation Frequency	f_{exc}	40 - 60	[Hz]
Test time	T	60	[s]
FPGA loop rate	Ts	20e-6	[s]
ATMD resonance	f_{ATMD}	50	[Hz]
Position feedback gain	γ	$4\pi^2 m_{\mathrm{ATMD}}({f_{exc}}^2 - {f_{ATMD}}^2)$	$[\mathrm{N}s^2/m\ ]$
Velocity feedback gain	β	-14	$[Ns/m]$
VCM reference current	i_{ref}	${k_{vcm}}^{-1}((\gamma(x_1 - x_2) + \beta(\dot{x}_1 - \dot{x}_2))$	[A]
"Control ON"	$f_{control}$	45 - 55	[Hz]
Low pass cut-off	f_{Lp}	200	
High pass cut-off	f_{Hp}	1	

The graphs of **Figure 10** present the experimental measurements of the shaker excitation and the shaker table acceleration for the test rig with passive TMD (black) and the actively controlled ATMD (red) for the purpose of comparison. The power consumption of the VCM is also plotted for the purpose of highlighting the efficiency of the control method.

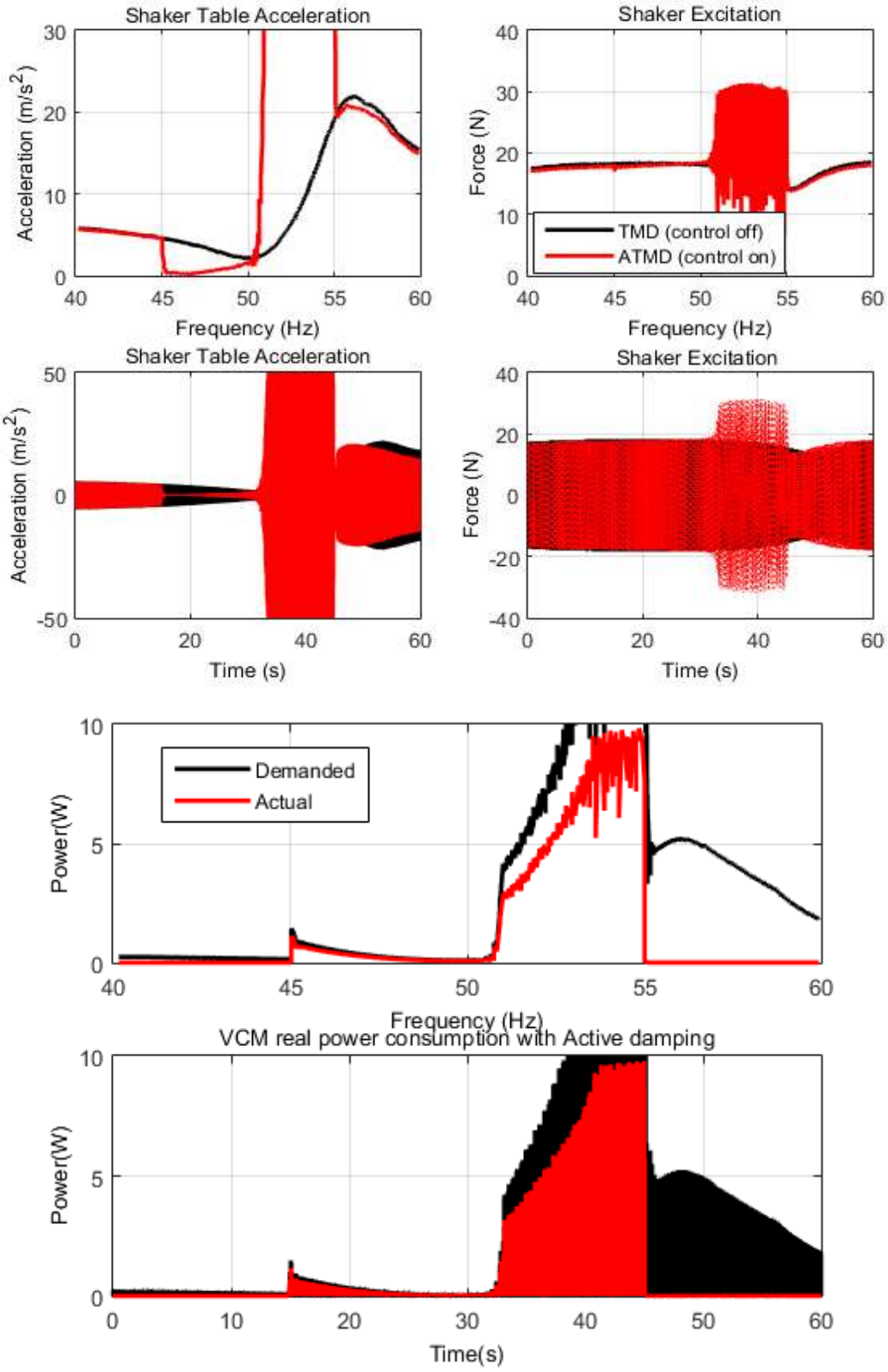

Figure 10. Experimental results of Test 1.

Referring to Figure 10, the top row of subplots on the left correspond to the magnitude of the shaker table acceleration and shaker force plotted against excitation frequency. The 2nd row of the subplots on the left shows the instantaneous acceleration and excitation force in against time. Note that the excitation frequency of the shaker is varied from 45Hz to 60Hz in 60 seconds. The figure on the right corresponds to the electrical power consumed by the VCM.

The shaker table acceleration with the passive case (black) is only attenuated at 50Hz which is the tuning frequency of the passive TMD. It is evident that the attenuation level doesn't cancel the vibration of the shaker table completely due to the damping in the VCM. The following discussion elaborates upon the active control (red) with ATMD whereby the response is analyzed in four different intervals.

1. [40-45]Hz: For the ATMD, the control is off in this interval and therefore the response of the shaker table acceleration is similar to that of the passive TMD response plotted in black. The current delivered to the VCM is zero in this interval due to the control being off. A small voltage appears across the terminals of the VCM in this interval due to the generated back EMF but this voltage is negligible.

2. [45-50]Hz: In the case of the passive TMD (black), the amplitude of the shaker table acceleration starts decreasing to reach a minimum at 50Hz due to resonance in the TMD. When control is on (red), the amplitude of the shaker table acceleration drops to minimum immediately at 45Hz due to the effect of the control action. As excitation frequency increases, it is revealed that the shaker table acceleration grows to larger amplitudes as soon as the excitation frequency approaches 50Hz. The maximum amplitudes power (1.8W) occurs at 45Hz. Theses amplitudes decrease gradually as the frequency reaches 50Hz.

3. [50-55]Hz: The control action is still on in this interval. The system becomes unstable after 50Hz and the amplitudes of the acceleration reach larger magnitudes as the frequency of excitation moves from 50Hz towards 55Hz. Similarly, the VCM voltage, current, and power reach larger values in this interval. The instability in the system caused higher demand in the VCM current due to the large acceleration amplitudes. This is evident in the graphs power where the actual power does not track the demanded ones. The source of instability in the control system is attributed to time delays resulting from filtering. The outcome of this test confirms the predictions obtained in the simulation earlier.

4. [50-55]Hz: This is the case when control is turned off in the system. No current is delivered to the VCM and hence the response of the shaker table acceleration is similar to that when the system is passive.

4.2. Test 2: Timed-delayed ATMD tuned at 55Hz

The theoretical findings of the effect of time delay on control stability were illustrated experimentally in implementation Test 1. Precisely, Test 1 showed that the control system becomes unstable when the excitation frequency is higher than the resonant frequency of the ATMD (50Hz) exactly similar to the observation in simulation results. It was also observed that the system only becomes unstable after the resonant frequency of the ATMD. Building upon this fact, one method of mitigating the effect of delays was proposed and simulated based on shifting the original resonance of the absorber up to 55Hz. The results of test 2 shown in **Figure 11** illustrate the success of the proposed method.

By examining the acceleration profile of the shaker table in **Figure 11** it is revealed that the active control succeeds in attenuating the vibration of the shaker table mass across the entire range of frequency range between 45Hz and 55Hz. The comparison between the power consumption of the VCM in this test with that of test 1 in **Error! Reference source not found.** shows that while this method is successful; more power is required than if the ATMD was originally tuned at 50Hz.

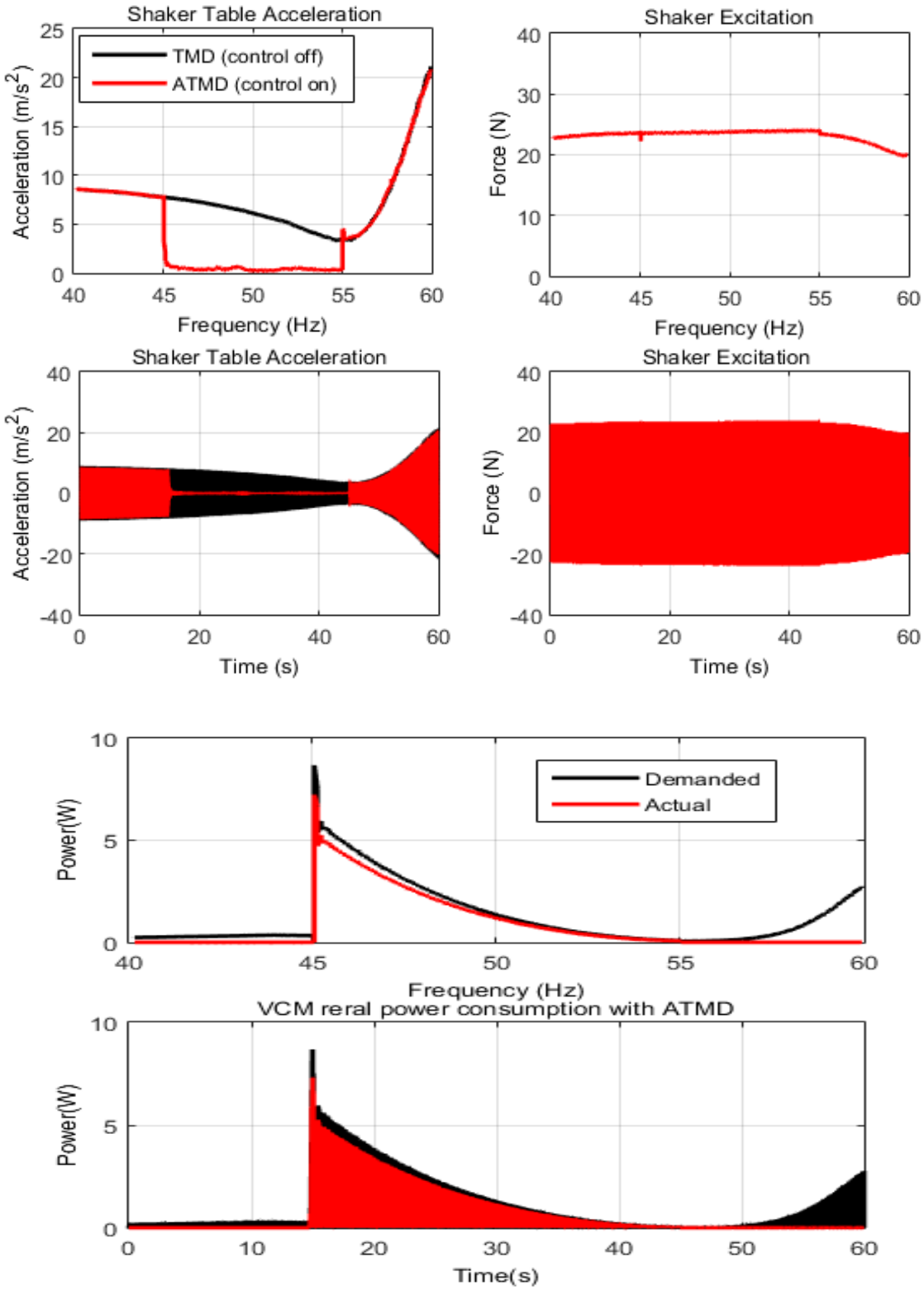

Figure 11. Experimental results of Test 2

4.3. Test 3: delay compensation

The compensation of time delays resulting from the filtering is achieved by adaptively altering the Low-Pass filter coefficients so that its cut-off frequency is chosen accordingly. The following schematic model represents that of Test 3.

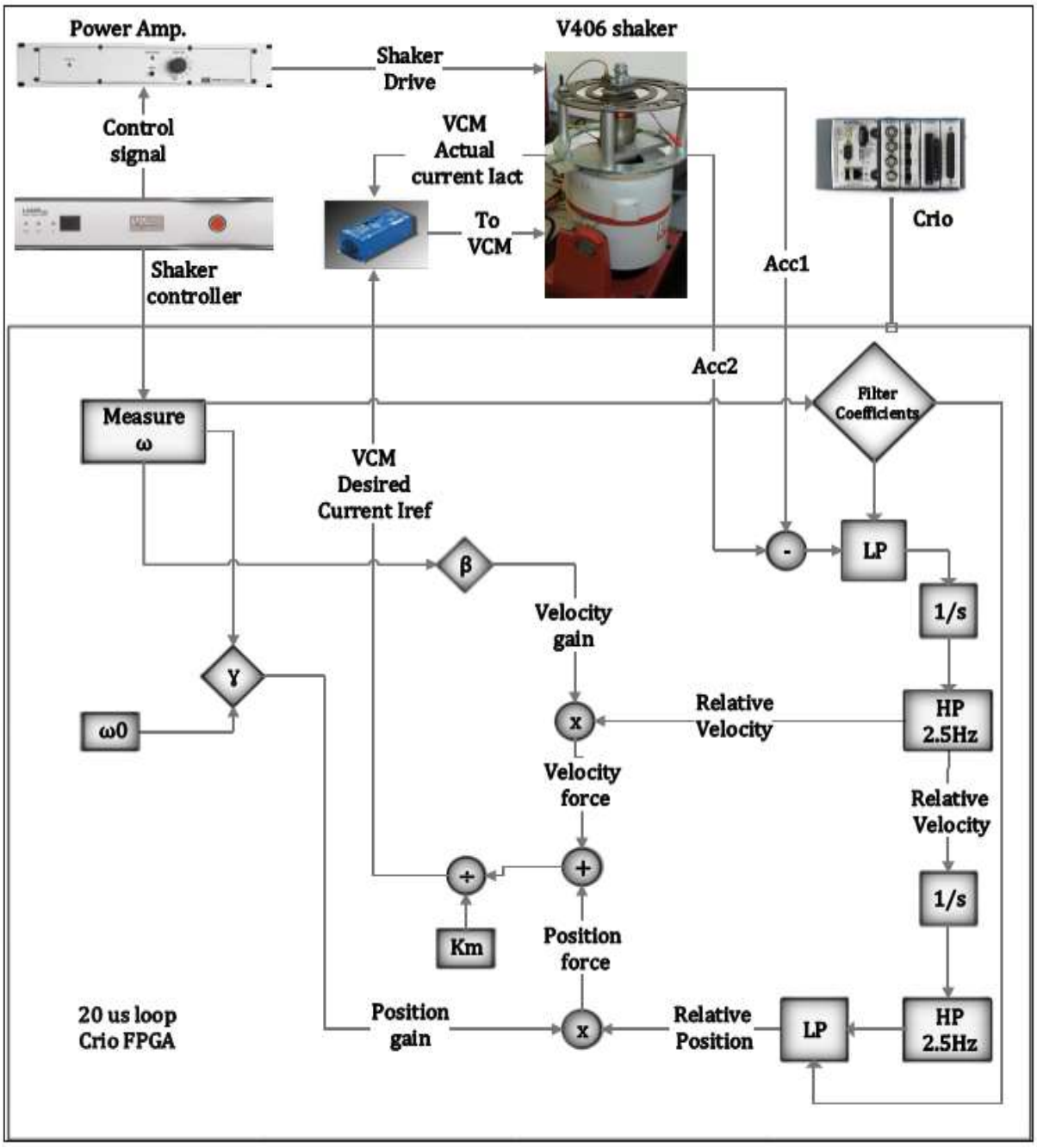

Figure 12. Schematic of the active damping control of Test 3

The values of **Table 3** are adopted in this experiment. The time and frequency domain results of this test are shown below.

Table 3. Parameters for Test 3

Parameter	Symbol	Value	Unit
Shaker Excitation	V_s	$4\ \sin 2\pi f_{exc} T$	[V]
Excitation Frequency	f_{exc}	40 - 60	[Hz]
Test time	T	60	[S]
FPGA loop rate	Ts	20e-6	[S]
ATMD resonance	f_{ATMD}	50	[Hz]
Position feedback gain	γ	$4\pi^2 m_{\mathrm{ATMD}}({f_{exc}}^2 - {f_{ATMD}}^2)$	$\mathrm{N}s^2/m$
Velocity feedback gain	β	$-(0.103{f_{exc}}^2 - 9.58f_{exc} + 208)$	$\mathrm{N}s/m$
VCM reference current	i_{ref}	${k_{vcm}}^{-1}((\gamma(x_1 - x_2) + \beta(\dot{x}_1 - \dot{x}_2))$	[A]
"Control ON"	$f_{control}$	45 - 55	[Hz]
Low pass cut-off	f_{Lp}	${f_{exc}}^2/f_{HP}$	
High pass cut-off	f_{Hp}	2.5	

The test was performed while catering for the delays in the system as described above. For the shaker table acceleration, the active damping succeeded in attenuating its vibration between 45Hz and 55Hz with stable control action across the entire range.

By comparing the results with that of Test 1, the results of Test 3 are shown in **Figure 13**. According to the results, it is illustrated that delays were the source of instability encountered in Test 1. The compensation of time delays has successfully improved the system response by maintaining stability of the control after 50Hz. In Test 2, delays were mitigated by shifting the ATMD original resonant frequency to 55Hz so that it located outside the range of operation. The method was successful however it incurred extra power consumption as explained previously. Following this method, the electrical power consumption in the VCM is improved.

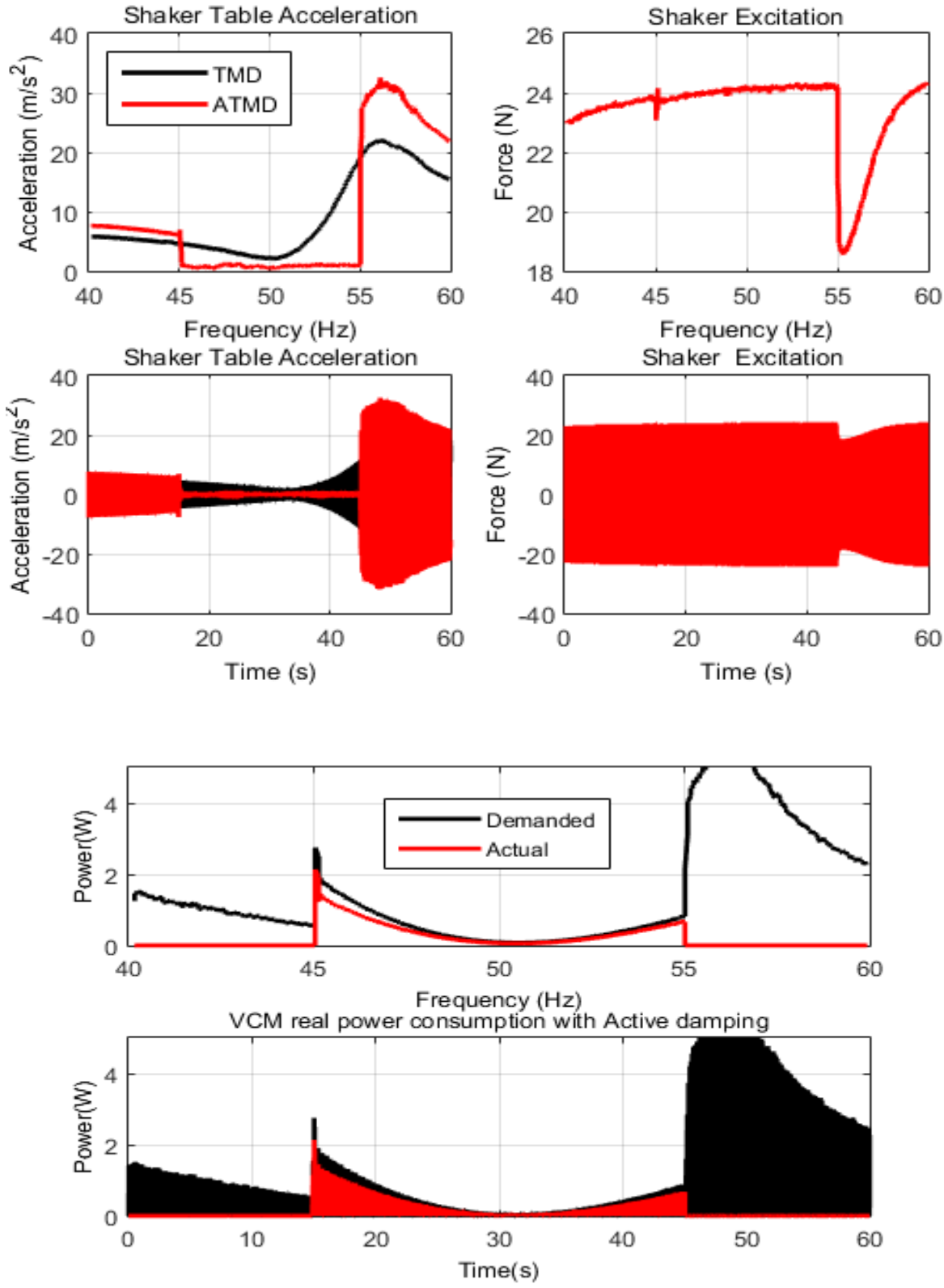

Figure 13. Experimental results of Test 3

5. Conclusion

In this work, an active vibration control method employing an electromagnetic ATMD with a voice coil actuator is employed for investigating a solution for the vibration problem in a Stirling machine with the aid of a scaled test rig. The experimental results with the test rig showed that the proposed active control law is capable of enhancing the frequency band of operation from 50±0.5Hz to between 45Hz-55Hz. A thorough theoretical and experimental investigation on the effect of time delays on control stability showed that after a critical time delay margin dependent of the excitation frequency the control system becomes unstable. Three methods for mitigating the effect of time delays on stability showed that it is possible to successfully mitigate the effect of time delays on the stability of the control system. The introduction of damping into that ATMD system improves the time delay margin allowing for more room of operation with a time-delayed ATMD. The second method incorporated re-tuning the original resonance of the ATMD which ensured stable control for excitation frequencies below the resonance of the ATMD. A third technique incorporating a dual-filtering technique of delay compensation provided a successful and less power-consuming solution compared to the other two. The proposed methods will not be only bound Stirling engine application specifically. In fact, it is useful for the compensation of the time delay effects in ATMD systems deployed in tall slender structures such as tall buildings, for effective mitigation of wind-induced vibrations.

References

[1] Walker G. 1980 *Stirling engines* Clarendon Press .

[2] Rao SS., 1990 *Mechanical vibrations* Addison-Wesley .

[3] Mead DJ. 1999 *Passive vibration control* Wiley .

[4] Ikeda Y. 2009 *Active and semi-active vibration control of buildings in Japan—Practical applications and verification* Structural Control and Health Monitoring 16 (7-8) 703-723 .

[5] De Roeck G, Degrande G, Lombaert G, Müller G. 2011 *A versatile active mass damper for structural vibration control* .

[6] Park K. Choi D. Ozer A. Kim S. Lee Y. Joo D. 2008 *A voice coil actuator driven active vibration isolation system with the consideration of flexible modes* Rev Sci Instrum 79 (6) 065106 .

[7] Liu Y. Wu W. 2013 *Active Vibration Isolation Using a Voice Coil Actuator with Absolute Velocity Feedback Control* International Journal of Automation and Smart Technology 3 (4) 221-226 .

[8] Qiu Z. Wu H. 2009 *Acceleration sensors based modal identification and active vibration control of flexible smart cantilever plate* Aerospace Science and Technology 13 (6) 277-290 .

[9] Thong YK. Woolfson MS. Crowe JA. Hayes-Gill BR. Jones DA. 2004 *Numerical double integration of acceleration measurements in noise* Measurement 36 (1) 73-92 .

[10] Liu B. Hu H. 2010 *Group delay induced instabilities and Hopf bifurcations, of a controlled double pendulum* Int J Non-Linear Mech 45 (4) 442-452 .

[11] Shao M. Chen W. 2012 *Active vibration control in a cantilever-like structure: a time delay compensation approach* J Vibrat Control 1077546312437802 .

[12] Jie Liu. Kefu Liu. and Hao Bai. 2005 *Application of a time-delayed control system in vibration suppression* Mechatronics and Automation, 2005 IEEE International Conference Anonymous .

[13] Cai G. Huang J. 2003 *Instantaneous optimal method for vibration control of linear sampled-data systems with time delay in control* J Sound Vibrat 262 (5) 1057-1071 .

[14] An F. Chen W. Shao M. 2014 *Dynamic behavior of time-delayed acceleration feedback controller for active vibration control of flexible structures* J Sound Vibrat 333 (20) 4789-4809 .

[15] Qiu Z. Han J. Zhang X. Wang Y. Wu Z. 2009 *Active vibration control of a flexible beam using a non-collocated acceleration sensor and piezoelectric patch actuator* J Sound Vibrat 326 (3–5) 438-455 .

[16] Hassan A. Torres-Perez A. Kaczmarczyk S. Picton P. 2015 *Active vibration control for a free piston Sirling engine generator using a voice coil actuator* mm (Modern Machinery) Science Journal (10.17973/MMSJ.2015_03_201503) 547 .

[17] Marques FA. Domingos A. Rade Sebastiao S. Cunha Jr. 2001 *Assessment of an active dynamic vibration absorber* Proceedings of IMAC-XIX: a conference on structural dynamics: February 5-8, 2001, Hyatt Orlando, Kissimmee, Florida Society for Experimental Mechanics Anonymous .

Appendix A

Coefficients of transfer function $W(s)$ shown in (6)

Numerator

$$b_5 = 0$$

$$b_4 = 0$$

$$b_3 = m_2 L_a$$

$$b_2 = -k_a^2 + c_2 k_p + c_2 R_a + k_2 L_a + \beta k_p - \gamma \tau k_p$$

$$b_1 = -k_a^2 + c_2 k_p + c_2 R_a + k_2 L_a + \beta k_p - \gamma \tau k_p$$

$$b_0 = k_2 k_p + k_2 R_a + \gamma k_p$$

Denominator

$$a_7 = 0$$

$$a_6 = 0$$

$$a_5 = m_1 m_2 L_a$$

$$a_4 = k_p m_1 m_2 + c_1 m_2 L_a + c_2 m_1 L_a + c_2 m_2 L_a + m_1 m_2 R_a - \beta \tau k_p m_1 - \beta \tau k_p m_2$$

$$a_3 = \beta k_p m_1 - k_a^2 m_2 - k_a^2 m_1 + \beta k_p m_2 + c_1 k_p m_2 + c_2 k_p m_1 + c_2 k_p m_2 + c_1 c_2 L_a + c_1 m_2 R_a + c_2 m_1 R_a + c_2 m_2 R_a + k_1 m_2 L_a + k_2 m_1 L_a + k_2 m_2 L_a$$

$$a_2 = -c_1 k_a^2 + \beta c_1 k_p + \gamma k_p m_1 + \gamma k_p m_2 + c_1 c_2 k_p + c_1 c_2 R_a + k_1 k_p m_2 + k_2 k_p m_1 + k_2 k_p m_2 + c_1 k_2 L_a + c_2 k_1 L_a + k_1 m_2 R_a + k_2 m_1 R_a + k_2 m_2 R_a$$

$$-\beta \tau c_1 k_p - \gamma \tau k_p m_1 - \gamma \tau k_p m_2$$

$$a_1 = -k_1 k_a^2 + \gamma c_1 k_p + \beta k_1 k_p + c_1 k_2 k_p + c_2 k_1 k_p + c_1 k_2 R_a + c_2 k_1 R_a + k_1 k_2 L_a - \gamma \tau k_1 k_p$$

$$-\gamma \tau c_1 k_p - \beta \tau k_1 k_p$$

$$a_0 = \gamma k_1 k_p + k_1 k_2 k_p + k_1 k_2 R_a$$